Chapter 11

The Investigation of Removing Direct Blue 15 Dye from Wastewater Using Magnetic *Luffa sponge* NPs

Hayrunnisa Nadaroglu, Semra Cicek, Hicran Onem and Azize Alayli Gungor

Additional information is available at the end of the chapter

http://dx.doi.org/10.5772/intechopen.73216

Abstract

In this study, loaded *Luffa sponge* membrane forms were modified with ZnO, Fe_3O_4, ZnO/Fe_3O_4 nanoparticles (NPs) to remove of Direct Blue 15 (DB15), which is a carcinogenic azo dye in aqueous solution. ZnO and Fe_3O_4 NPs were synthesized using purified peroxidase enzymes from *Euphorbia amygdaloides* using green synthesis method. Adsorption of DB15 azo dyes was separately studied with membrane forms (LS-pure, LS-ZnO, LS-Fe_3O_4, and LS-ZnO/Fe_3O_4). Optimum contact time, optimum pH, optimum temperature, optimum dye concentration, and optimum LS amount were found as 45 min, pH 8.0, 20°C, 200 mg/L, and 0.025 g in line with the optimization studies, respectively. The obtained membrane forms were characterized using SEM, FT-IR, and XRD techniques. According to obtained results, NPs loaded LS membrane forms are promising in removal of DB15 from textile wastewater contaminated water.

Keywords: Fe_3O_4, ZnO, nanoremediation, *Luffa sponge*, Direct Blue 15

1. Introduction

There are more than 3000 different dyes available and half of them belong to the azo dyes compounds class [1]. Azo dyes are the most frequently used dyes in textile industry and are characterized by the presence of one or more azo linkages (—N=N—), usually in number of one or four, linked to phenyl and naphthyl radicals, which are usually replaced with some combinations of functional groups including: amino (—NH_2), chlorine (—Cl), hydroxyl (—OH), methyl (—CH_3), nitro (—NO_2), sulfonic acid (—SO_3H), and sodium salts (—SO_3Na) [2–4]. These compounds can lead to significant ecological problems because of the creation

of carcinogenic or mutagenic compounds [5–7]. Several azo dyes have been described to lead human bladder cancer, splenic sarcomas, and hepatocarcinoma, because azo dye reduction in the intestinal tract release aromatic amines which are absorbed by the intestine and excreted in the urine [8]. The acute toxicity of azo dyes, with respect to the criteria of the European Union for the sorting of unsafe substances, is low and the values of LD_{50} are 250–2000 mg/kg body weight [9, 10].

The textile dyes can be removed by using physical, chemical, and biological methods [11]. Nevertheless, most of these methods, which simply accumulate or concentrate the dyes, and trigger secondary contamination, resulted in the extreme usage of chemical materials [11, 12].

Because of nanoparticles' features arising from size effect, nanotechnology has emerged in many scientific and industrial fields [13, 14]. It involves studies of measurement, modeling, and manipulation of substance in nanoscale. Nanoremediation is economic and has improved overall efficiency of fragmentation process. Potential catalytic activity of Au, Ag, Pd, Mg, Cu, Zn, and Fe nanoparticles have been reported for degradation of some aqueous cationic and anionic dyes [14–18]. Researchers studied degradation of Methyl Orange, Sunset Yellow, Acid Blue A azo dyes using zero valent iron nanoparticles (NZVI) with diameters between 20 and 110 nm. Methyl Orange, Sunset Yellow, Acid Red A were removed using solution prepared with 2 g NZVI rate of 79.9, 98.9, and 98.8, respectively [19].

However, nanoparticles are left in the ecosystem after their use in the removal of environmental contaminants. Thus, nanoparticles immobilized on a support material are to the fore for environmental remediation [20, 21]. LS is eco-friendly, cost effective, easy to use matrix material successfully used as a biotechnological tool for variety of systems, purposes and applications. LS immobilized cell systems have efficiently studied toward biofilm development for remediation of domestic and industrial wastewater containing toxic metal, paint, chlorinated compounds [22, 32].

In this study, ZnO and Fe_3O_4 nanoparticles were obtained by catalyzing using purified peroxidase enzymes from *Euphorbia amygdaloides* with green synthesis method. Membrane forms have been created by immobilizing the obtained nanoparticles on LS support material. Carcinogenic DB15 azo dye was used to evaluate effectiveness of ones to remove dye (molecular structure of DB15 shown in **Figure 1**). Optimum contact time, pH, temperature, and concentration of dye were analyzed using UV-visible spectrometry. The resulting adsorbents (LS-pure, LS-ZnO,

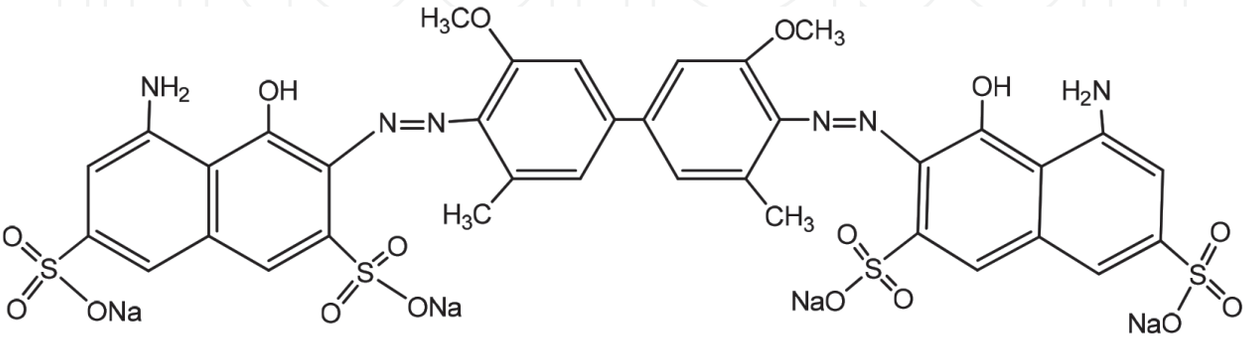

Figure 1. Molecular structure of DB15.

LS-Fe_3O_4, and LS-ZnO/Fe_3O_4) were characterized by SEM, FT-IR, and XRD. Also, adsorption isotherms and kinetics and thermodynamics of these membrane forms were investigated.

2. Materials and methods

2.1. Materials

Direct Blue 15 (CAS no: 2429-74-5), $FeCl_2$, $ZnCI_2$, and other chemicals were purchased from Sigma-Aldrich. Euphorbia (*Euphorbia amygdaloides*) was collected from near the town of Hasankale of Erzurum. Also, LS which is fruit of *Luffa cylindrica* was obtained from a local point of spices sale in Erzurum, Turkey, and they were identified with the helping of taxonomists. All solutions were made in deionized water.

2.2. Green synthesis of Fe_3O_4 and ZnO nanoparticles

2.2.1. Collection of plant sample and preparation of plants extract

Plants (*Euphorbia amygdaloides*) were collected from Hasankale town of Erzurum city. They were washed with distilled water several times for cleaning dust and soil on plants. Then, plants were cut into small pieces. Small pieces (50 g) were thoroughly shattered to form a homogeneous mixture in blender using 250 mL, 10 mM sodium phosphate buffer (pH 6.0). Then, it was centrifuged at 5000×*g* for 10 min and the supernatant was used for enzyme purification [23].

2.2.2. Partial purification of the peroxidase enzyme with ammonium sulfate precipitation

Prepared Euphorbia (*Euphorbia amygdaloides*) plant homogenate was saturated from 60 to 80% with ammonium sulfate, then the peroxidase enzyme was precipitated by centrifuged at 8000×*g*, 10 min. Obtained precipitate was dissolved at 10 mM sodium phosphate buffer (pH 6.0) and was incubated at 4°C for further analysis [23].

2.2.3. Peroxidase enzyme activity test

Determination of peroxidase activity was made by substrate of 1 mM 2,2′-azino-bis(3-ethylbenzthiazoline-sulfonic acid) diammonium salt (ABST) prepared in 0.1 M phosphate buffer at pH 6. For this purpose, 2.8 mL ABST was transferred to a test tube, and then the reaction mixture was formed by the addition 100 μL of 80% enzyme and 100 μL of 3.2 mM H_2O_2 solution into the test tube. The change in absorbance was monitored at 412 nm using UV–Visible spectrophotometer at 1 min intervals for 3 min. Blank test tube was prepared using distilled water instead of enzyme in the reaction mixture.

2.2.4. Synthesis of Fe_3O_4 and ZnO nanoparticles

100 μL of purified peroxidase enzyme from Euphorbia (*Euphorbia amygdaloides*) plant were added in sample $FeCl_2$ of solution (2.9 mL, 10 mM) and incubated in a closed space for 4 h.

The solution was becoming dark red, which indicates the presence of Fe_3O_4 nanoparticles. The same procedures were repeated using 2.9 mL of 10 mM $ZnCl_2$ solution to obtain ZnO nanoparticles. The solution became a white turbid state indicating the presence of ZnO nanoparticles. Then, water was removed by the help of an evaporator, and synthesized iron and zinc oxide nanoparticles were dried at 70°C for 24 h.

2.2.5. Characterization of Fe_3O_4 and ZnO nanoparticles

Synthesized Fe_3O_4 and ZnO NPs were characterized by scanning at range of 200–1000 nm by using UV-Vis spectrophotometer (Epoch nanodrop spectrophotometer). Determination of topography for Fe_3O_4 and ZnO nanoparticles was performed by SEM (Scanning Electron Microscope). In addition, XRD analysis (X-ray diffraction analysis) and FT-IR (Fourier transform infrared spectroscopy) were performed for Fe_3O_4 and ZnO NPs.

Contact time, pH, temperature, and metal ion concentration were determined for the purpose of optimization synthesized Fe_3O_4 and ZnO NPs. For determination of the optimum contact time, samples were spectrophotometrically measured between 0 and 240 min with 3 min intervals. Synthesis of Fe_3O_4 and ZnO NPs was performed in sodium phosphate buffer at pH 2.0–3.0, sodium acetate buffer at pH 4.0–6.0, sodium phosphate buffer at pH 7.0–8.0 and sodium carbonate buffer at pH 9.0–11.0 and the values of absorbance were measured. pH was adjusted by using 0.1 N HCl and 0.1 N NaOH. Synthesis of NPs was separately carried out from 10° to 90°C, respectively, and changes in absorbants of the samples were measured. Synthesis of NPs was performed by using related solution at 0.5, 1, 3, 5, and 7 mM and the absorbance of samples was measured. All measurements were performed by UV–VIS spectrophotometer and deionized water was used for blank sample.

2.3. Preparation of LS material, immobilization of nanoparticles procedure

Dried LS material was made into small pieces and was autoclaved for 20 min to soften the fibrous structure. Then, it was transformed into dough using blender. It was incubated for 4 h with 1 N NaOH at 80°C. Then, the fibers were collected and were thoroughly washed with distilled water until NaOH is resolved. About 0.1% hypochlorite was used for decoloration of washed fibers and then, they were washed with distilled water. Fibers with the length of 10–50 μm were collected and were dispersed with distilled water to form a suspension form. The suspension was filtered under aseptic conditions using filter paper and obtained LS fibers were dried on filter paper at 40°C for 4 h [24]. Immobilization was performed by treatment solutions containing Fe_3O_4 and ZnO NPs with LS which was pretreated in ultrasonic bath for 1 h. Then, the obtained membrane forms (LS-pure, LS-ZnO, LS-Fe_3O_4, LS-ZnO/Fe_3O_4) was dried in oven for 2 h.

2.4. Azo dye remediation

The prepared membranes were used for decolorization of DB15 solution which was prepared in the laboratory. Synthetic wastewater was prepared by dissolving DB15 dye. A calibration

curve was prepared in the range 0–40 ng/cm^3 of DB15. The reaction mixture was prepared by adding membrane forms and in flasks containing 50 mL volume DB15 dye solution. The samples were taken out from the flasks periodically with a micropipette and were centrifuged at 5000 rpm for 10 min. The supernatant solutions were filtered with 0.45 mm filters. Then, the concentration of DB15 was measured with a UV–VIS spectrophotometer at λ = 596 nm. Scanning electron microscopy (SEM) was used to examine the surface of the adsorbents before and after dye adsorption (JEOL JSM-6400 SEM) and FTIR, XRD were performed for dye adsorption. Optimum contact time, pH, temperature, concentration of dye to determine optimal conditions for the decolorization of DB15 azo dye were analyzed using UV-Visible spectrophotometer.

The amounts of the dyes adsorbed onto LS-pure, LS-ZnO, LS-Fe_3O_4, and LS-ZnO/Fe_3O_4 (q_e in mg/g) were calculated from the equation:

$$q_e = \frac{(C_o - C_e) \times V}{m} \quad (1)$$

where C_o and C_e are the initial and equilibrium concentrations of dye in solution (mg/L); V is the volume of solution (L) and m is the mass of adsorbent (g).

2.5. Adsorption isotherms

Plots of ln(C/C_o) and time were drawn to estimate rate constants (k values) for decolorization as a function of dye concentration, where C_o and C represent remaining color intensity at the start of the experiment (zero time) and at any time t, respectively, for various fixed concentrations of dye.

3. Results and discussion

3.1. Partial obtaining peroxidase enzyme from *Euphorbia amygdaloides* plant

The data obtained in the purification process of peroxidase enzyme are given in **Table 1**.

There are many studies on the purification of peroxidase enzyme in the literature. Plants such as wheat seeds, barley and wheat, soybeans, fava beans, sorghum, watermelon seeds, red beets, cotton, pearl millet seedlings, Asian rice, lettuce, wild radish, and pearl barley hybrids were used for the purification of peroxidase enzyme [25–29].

Peroxidase enzyme was purified by ammonium sulfate precipitation from *Euphorbia amygdaloides* plant with CM-cellulose ion exchange chromatography and Sephacryl S-100 gel filtration chromatography. According to the data obtained in 75% ammonium sulfate precipitation step, the enzyme was purified with purification coefficient of 6.4 and 51.6 for 10 mL volume [23]. In our study, the enzyme was purified with a purification coefficient of 149.5 and a yield of 29.5 for 20 mL volume, according to the order of 60–80% ammonium sulfate precipitation step.

Enzyme fraction	Volume (mL)	Activity (EU/mL)	Total activity (EU) 10^3/%	Protein (mg protein) (mL)	Specific activity (EU/mg)	Purification coefficient (EU/mg)
Crude extract	50	236.4 ± 1.0	11.82/100	$3.82\times10^2\pm$ 0.7	0.62	—
$(NH_4)_2SO_4$ (60–80%)	20	174.3 ± 1.02	3.49/29.5	1.88 ± 0.16	92.71	149.54

Table 1. Purification process of peroxidase enzyme from *Euphorbia amygdaloides* plant.

3.2. Characterization of Fe_3O_4 and ZnO NPs

The results of the optimization studies for the green synthesis of nanoparticles are given in **Table 2**.

No research has been found in the literature on the green synthesis of Fe_3O_4 and ZnO NPs from the *Euphorbia amygdaloides* plant. *Euphorbia milii* was used for the synthesis of ZnO nanoparticles [30]. A study on the green synthesis of the Fe_3O_4 nanoparticle using the *Euphorbia amygdaloides* plant is not available in the literature. However, studies on the green synthesis of Pd/Fe_3O_4 nanoparticles using *Euphorbia condylocarpa M. bieb* root extract and *Euphorbia stracheyi Boiss* root extract have been carried out [31]. Our study provides a contribution to the literature. The highest peak in the optical absorption spectrum of the ZnO nanoparticles synthesized by pulsed laser ablation was at 300 nm [32]. In our study, the highest peak value of ZnO nanoparticles was read at 304 nm (**Table 2**). The sharpness of ZnO absorption indicates the uniform nanoparticle distribution [33, 34]. Fe_3O_4 nanoparticles exhibit an absorption band in the range of 330–450 nm of the UV–Vis spectrum in the literature and Fe_3O_4 nanoparticles peak observed at 330 nm in a work [35]. The highest peak value of the Fe_3O_4 nanoparticles used in our study was read as 481 nm. This range is above the range available in the literature. Nagarajan and Kuppusamy [36] studied the optical properties of ZnO nanoparticles obtained from marine algae of Mannar Bay in India. They did not observe any peak between pH 5.0–7.0 and pH 9.0–10.0 in their pH optimization studies. The maximum yield was obtained at pH 8.0. In our study, pH 6.0 was determined as the optimum pH for ZnO nanoparticle synthesis. Optimum pH for Fe_3O_4 nanoparticles is found at 8.0. Manouchehr et al. [37] reported that they performed the synthesis of Fe_3O_4 nanoparticles in the pH 7.0–9.0 environment. These values are close to the values we have obtained in our study. While the highest absorbance values were obtained at a concentration of 5 mM $ZnCl_2$ in the synthesis of ZnO nanoparticles, the highest absorbance values were obtained at a concentration of 1 mM $FeCl_2$-Fe_2Cl_3 in the synthesis of Fe_3O_4 nanoparticles.

Nanoparticle	Wavelength (nm)	Contact time (h)	pH	Temperature (°C)	Metal ion concentration (mM)
ZnO	304	4	6.0	60	5
Fe_3O_4	481	4	8.0	30	1

Table 2. The results of the optimization studies for the green synthesis of nanoparticles.

http://dx.doi.org/10.5772/intechopen.73216

SEM (scanning electron microscope) basically works on the basis of obtaining the images of the surface morphology which are scanned with the help of electrons. The electrons sourced from tungsten tip are sent to the surface to be scanned. After that, the emitted electrons are captured by the detector and the image is formed. SEM analysis images of ZnO and Fe_3O_4 nanoparticles in this study taken in this way are shown in **Figure 2**. The SEM image recorded for the Fe_3O_4 nanoparticle structure resembled a dust particle, suggesting that it may be a soft structure. It has been determined that these nanoparticle structures obtained by the surface characterization process have an average size of 30–80 nm. The SEM image for ZnO nanoparticle was taken at 5 μm. In this image, the nanoparticle structure exhibits a wavier surface. Generally, the liquid containing peroxidase enzyme prevents the formation of ZnO nanoparticle formations composed of dust and flake-like structures. However, it appears that the powder and flake structures combine in some regions and exhibit a wavy appearance after this enzyme liquid is evaporated. After the surface characterization analysis of ZnO nanoparticles, it was found that these structures vary between 60 and 80 nm on average.

The Fourier Transform Infrared Spectrophotometer (FTIR) is used to determine the bond formation between the elements present in the structure to be measured. In this direction, the structural formation that the sample possesses can be understood by measuring the vibrations of the bond occurrences in the structure at certain frequencies. This helps in the determination of the functional groups in the material being measured. The FT-IR spectrums of ZnO and Fe_3O_4 nanoparticles are given in **Figure 3**.

When looking at **Figure 3A**, it is possible to observe the absorbance at 510–564 cm^{-1}, which is indicative of Zn-O band formation in this analysis which was carried out to detect the biomolecule by revealing the stabilization ability and bandwidth of the metal nanoparticles synthesized by green synthesis [38]. Geetha et al. [30] synthesized ZnO nanoparticles by green synthesis using the *Euphorbia spindle* plant. They applied FT-IR analysis in their characterization studies

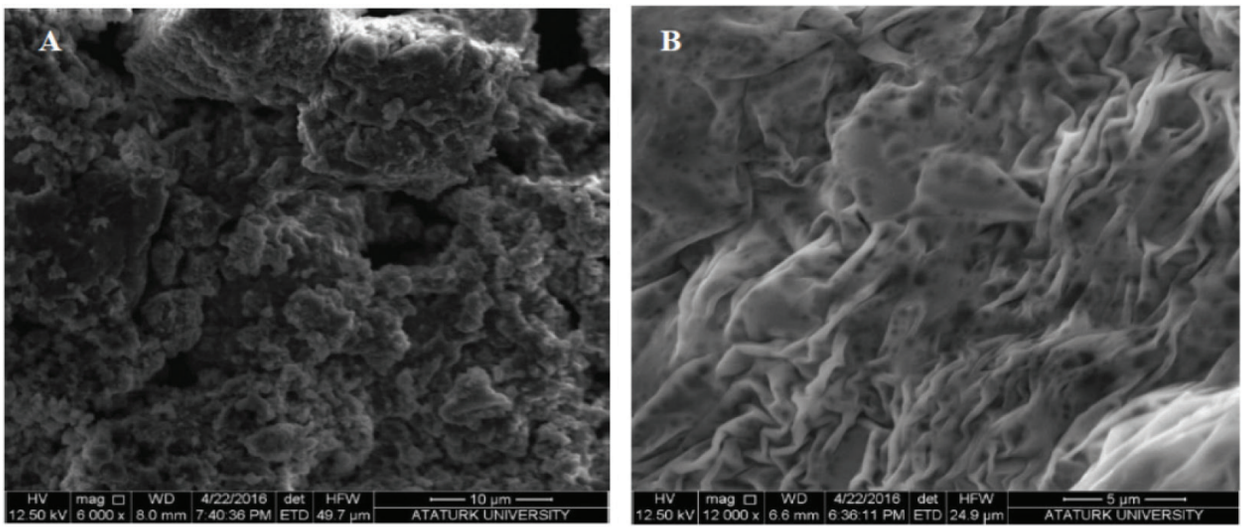

Figure 2. SEM analysis images of ZnO and Fe_3O_4 nanoparticles.

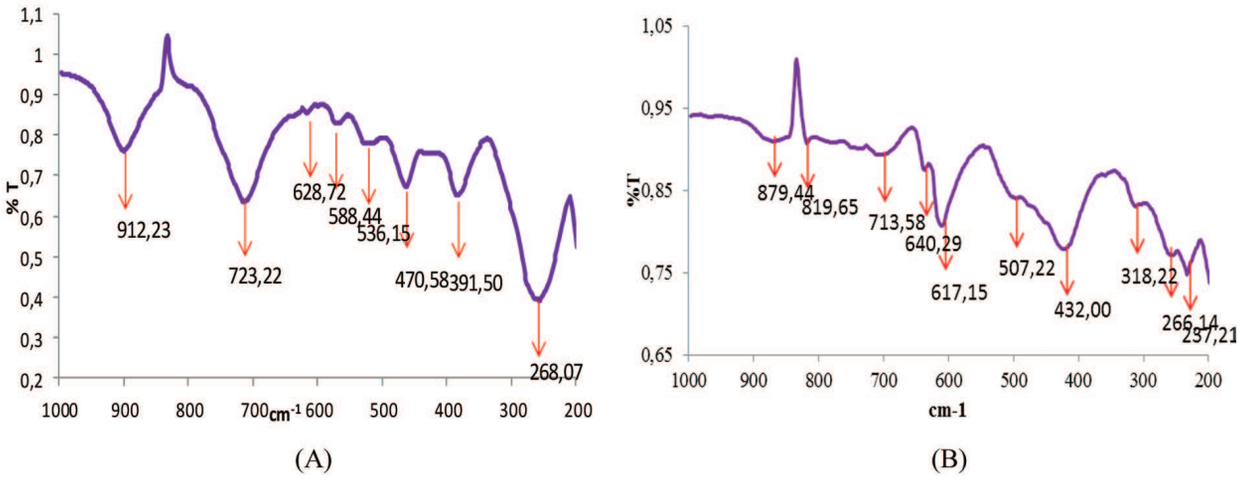

Figure 3. FTIR spectrum of (A) ZnO and (B) Fe_3O_4 nanoparticle.

in the range of 400–4500 cm^{-1}. The researchers noted that the observed transmittance band at 435 cm^{-1} corresponds to ZnO bonding, confirming the formation of ZnO particles.

In the FT-IR spectrum of the Fe_3O_4 nanoparticle structure shown in **Figure 3B**, there are oscillations of bond structures that oxygen forms with iron. It is known that this nanoparticle structure oscillates between 200 and 650 cm^{-1}. In this direction, as shown in the graph, the Fe_3O_4 nanoparticle structure obtained by green synthesis exhibited oscillations indicating specific bonds between iron and oxygen elements between 256 cm and 636 cm^{-1}.

XRD (X-ray diffraction) method was used for the analysis of crystallized structures of nanoparticles used in the study. In this method, since the diffraction pattern to be produced by each structure will be different, the planar structure of the elements arranged symmetrically or periodically can be determined. The graphs obtained by XRD analysis of ZnO and Fe_3O_4 nanoparticles are given in **Figure 4**.

Plots of 100, 002, 101, 102, 110, 103, 200, 112, 201, 004, and 202 were determined in the XRD analysis graph to show the crystallized structure of the ZnO nanoparticle. ZnO nanoparticle

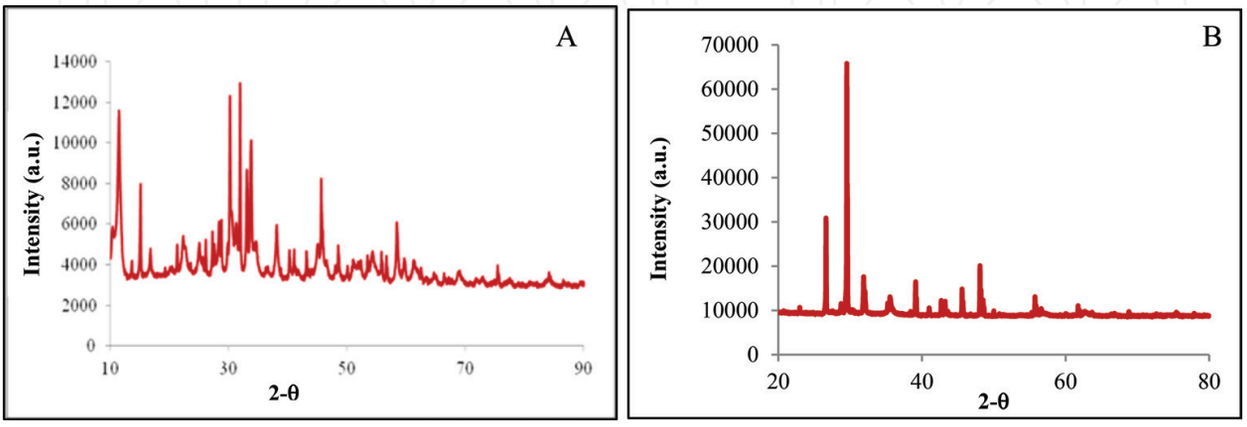

Figure 4. XRD spectrum for (A) ZnO and (B) Fe_3O_4 nanoparticle.

structures are located at 2θ angles of 31.77, 34.40, 36.22, 47.61, 56.58, 62.85, 66.41, 67.93, 69.08, 72.54, and 76.85° corresponding to the plane distances of the atoms present in the structure of the nanoparticle. In this case, the XRD chart confirms that the nanoparticle we are analyzing is a ZnO nanoparticle.

Nearly all of the characterization studies for ZnO nanoparticles synthesized by different methods in the literature are discussed according to XRD analysis results. In the analyses, the planes are generally observed at the highest peak 101 with the planes of 100, 002, 101, 102, 110, 103, 112 [30, 39]. In parallel with these studies in the XRD spectrum we obtained in our study, the 101 plane has the highest peak.

The peaks obtained in the XRD spectrum of the Fe_3O_4 nanoparticles reveal that the desired nanoparticle structure is obtained in the green synthesis process carried out. 2θ values specific to this nanoparticle were determined as 30, 33, 44, 53, 56, and 62°.The distances between the planes determined in this direction are 220, 311, 400, 422, 511, and 440 respectively. In the light of this information, it is determined that the Fe_3O_4 nanoparticle structure is in a spherical crystal structure.

3.3. Immobilization efficiency

The data obtained for the immobilization of nanoparticles on the LS are given in **Table 3**.

3.4. Adsorption studies

Analytical methods used for quantitative analysis require calibration. Calibration is a process for accurately determining the relationship between the signal measured at the output of any device and the concentration of the material causing the signal. The curve obtained is a straight line. Since the calibration curve R^2 value is 0.9941, the slope is assumed to be 0.0094.

As seen in **Figure 5**, the DB15 azo dye had value of about qe = 80 mg/L with all membrane forms in the first 15 min. Measurements at 30, 45, and 60 min resulted in 80–100 mg/L qe. However, since the highest values were noted at 45 min, optimum contact time for this azo dye was accepted as 45 min. ZnO and Fe_3O_4 NPs have been used to study the remodeling of many azo dyes [40, 41]. The LS-ZnO membrane form provided slightly lower adsorption compared to the LS-Fe_3O_4 NPs membrane form. The highest adsorption was obtained with LS-ZnO/Fe_3O_4 NPs membrane form.

Nanoparticle solution	Wavelength (nm)	Absorbance before immobilization	Absorbance after immobilization	% immobilization
ZnO	304	0.147	0.012	91.83
Fe_3O_4	481	0.188	0.015	92.02
ZnO/Fe_3O_4	209	0.202	0.014	93.07

Table 3. Data of immobilization efficiency.

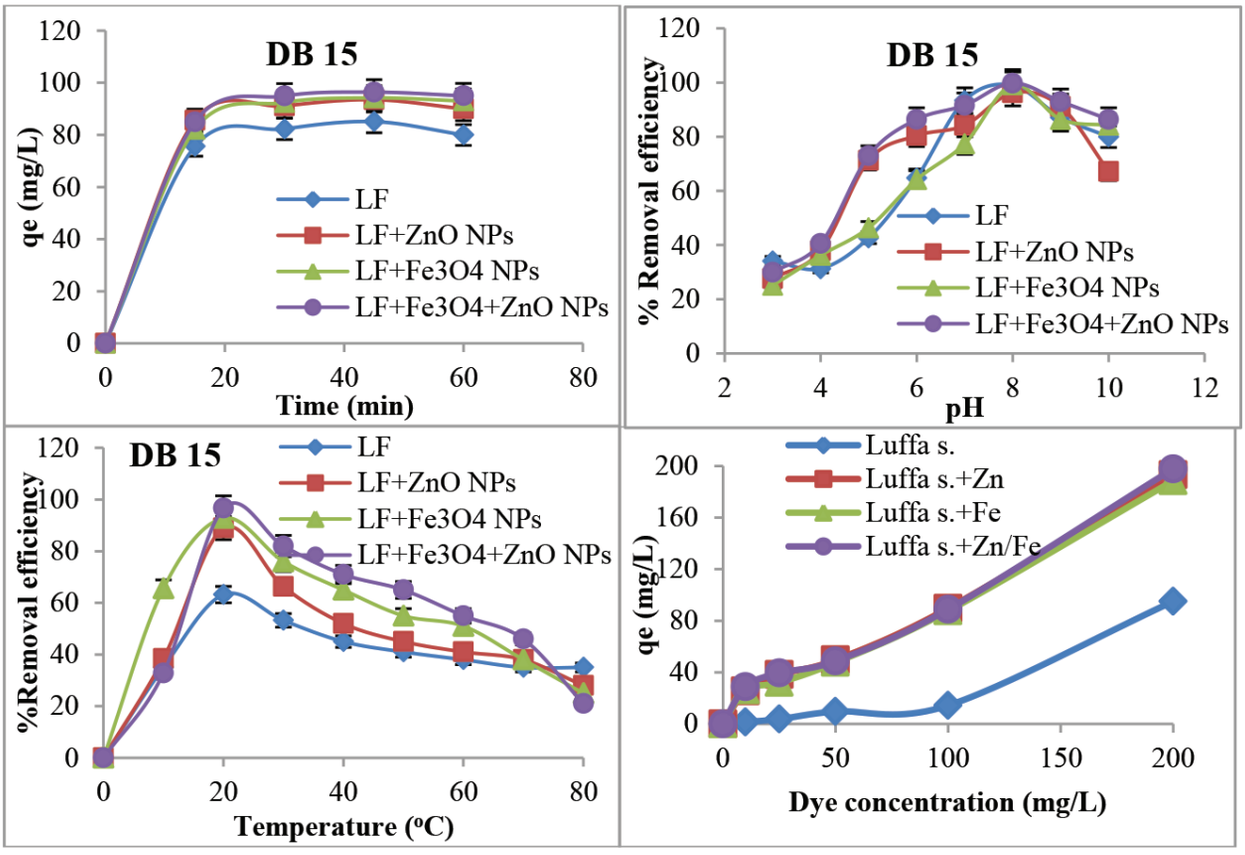

Figure 5. The effects of contact time, pH, temperature and dye concentration on the adsorption of the DB15 azo dye solution with the formed membrane forms.

Maximum adsorption peaks were observed at pH 8.0 in the spectrophotometric measurements performed on pH optimizations for the adsorption of DB15 azo dye solution at 50 mg/L concentration with the formed membrane forms. According to adsorption data obtained with LS-ZnO NPs and LS-Fe_3O_4 NPs membrane forms in pH 7.0 medium, pure LS membrane form provides a more effective adsorption in this pH environment. However, at pH 7.0, the same adsorption data were observed for LS-ZnO/Fe_3O_4 NPs and pure LS membrane forms (**Figure 5**).

In some studies performed onto Fenton process, a high decolorization rate was achieved for DB15 azo dye in highly acidic media such as pH 3.0 and 4.0 [42, 43]. Providing maximum yield in alkaline environment such as pH 8.0 near neutral with the formed membrane forms is advantageous in terms of operating.

The adsorption of the DB15 azo dye solution with membrane form exhibited the highest adsorption peaks at 20°C. However, when the temperature was gradually increased above 20°C, the adsorption with membrane forms showed an inverse proportion and gradually decreased. This result is quite advantageous in terms of the industrial application because the approximate temperature of 20°C is accepted as the optimum value.

In the work for the degradation of DB15 azo dye using copper hydroxide nitrate as a catalyst by wet peroxide oxidation, it has been reported that degradation activity of 85 and 90% of this dye is obtained after 10 and 60 min at 60°C [44]. In another study, remediation of DB15 azo dye was studied with Fenton reaction, and in this study, the degradation efficiency of the system was increased in parallel with the temperature increasing from 20 to 40°C [42]. The temperatures in these studies are very high and cause extra energy consumption and therefore financial loss. In this respect, the membrane forms proposed in our work offer advantages at 20°C with effective performance.

When **Figure 6** is examined, the adsorption of concentration of 200 mg/L DB15 azo dye solution prepared with the membrane forms had the highest value. The adsorption of the DB15 azo dye solution prepared at the concentration of 200 mg/L with LS-ZnO NPs, LS-Fe_3O_4 NPs, and LS-ZnO/Fe_3O_4 NPs membrane forms showed the highest values were measured according to the adsorption of azo dye solutions prepared at other concentrations (10, 25, 50, and 100 mg/L). The use of nanoparticles has affected adsorption quite positively. Pure LS membrane form showed very low efficiency in dye adsorption compared to nanoparticle loaded membrane forms.

Adsorption values were read close to each other in the adsorption study of the DB15 azo dye solution with membrane forms formed with LS quantities of 0.025, 0.05, 0.1, 0.3, and 0.5 g. In the adsorption study of azo dye solution with nanoparticle-loaded membrane forms formed with all LS quantities used in the experiment, higher adsorption values were obtained compared to the pure LS membrane form used in the same amount. The highest percentage of recovery was obtained with 0.025 g LS (**Figure 6**). Kesraoui et al. [45] conducted biosorption of the Alpasit Blue with LS. In this study, maximum efficiency was obtained with 1 g LS fibrils after 2 h in pH 2.0 medium with 20mg/L concentration dye. In our study, the highest yield was achieved with an adsorbent amount of 0.025 g. In addition, nanoparticle loading has made this more efficient.

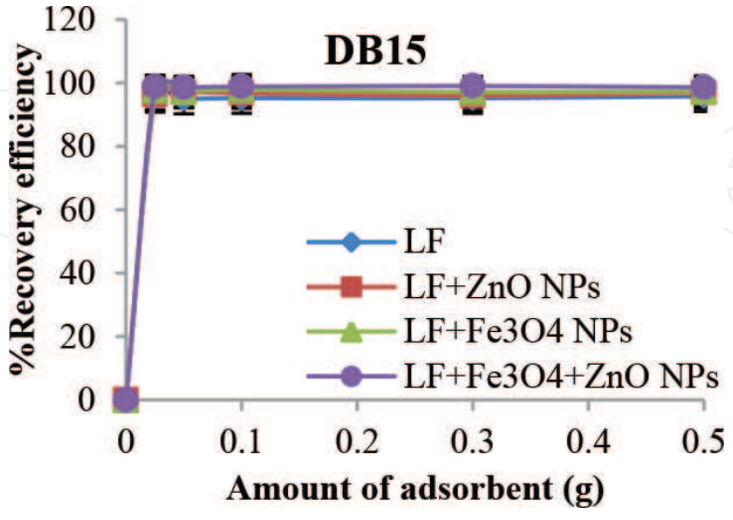

Figure 6. Effect of amount of adsorbent on adsorption with membrane forms formed by DB15 azo dye.

3.5. Characterization studies of dye absorption with prepared nanoparticle loaded membrane forms

SEM images for the adsorption of DB15 azo dye with the membrane forms obtained in the study are given in **Figure 7**. SEM images were taken at a size of 10 μm at 8000× magnification. It is seen that the DB15 azo dye has drained the membrane forms like a cover.

As shown in **Figure 8**, membrane forms formed with LS material exhibit significant peaks, especially at permeability of 1000 cm^{-1}. At the same time, certain peaks were observed at about 500 and around 3350 cm^{-1}. In fact, FT-IR bands specific to the cellulose structure of LS seen here. C—H bands and —OH groups are found at around 3350 and 2800–2900 cm^{-1} [46, 47]. In the adsorption of DB15 azo dye with LS membrane forms, FT-IR bands were observed especially for Fe_3O_4 nanoparticle-loaded membrane forms. ZnO NPs loaded membrane had higher permeability to dye adsorption than other membrane types.

The XRD spectrum of the LS membrane form showed peaks at 2θ = 15, 20, and 38 areas. The peak intensity is above 30,000 in the area 2θ = 20. However, in the XRD spectrum of DB15 azo dye adsorption with this membrane form, the 2θ = 20 area shifted to 2θ = 22 and the peak intensity approached 60.000 in this area. In addition, additional peak was observed at 2θ = 35, 38, 43, and 50 areas. Nanoparticle-loaded membrane forms exhibited significant changes in XRD spectra when DB15 azo dye adsorbed with these membrane forms. These membrane forms exhibited very low XRD peaks compared to the pure LS membrane form, but they exhibited very high XRD peaks especially in the 2θ = 15 and 20 areas after dye adsorption. A distinctive feature of ZnO and Fe_3O_4 NPs in the adsorption of this azo dye was not observed in the XRD spectrum. The values were very close to each other (**Figure 8**) [47–49].

3.6. Langmuir and Freundlich adsorption isotherm studies

The following Langmuir isotherm equation is used to plot Langmuir adsorption isotherm graphs for the adsorption of DB15 azo dye with the membrane forms in this study. The correlation between $\frac{Ce}{qe}$ and C_e calculated from experimental results is given in **Figure 9**.

$$\frac{Ce}{q_e} = \frac{1}{k V_m} + \frac{C_e}{V_m} \tag{2}$$

Using the following Freundlich adsorption isotherm equation, Freundlich adsorption isotherm graph for the adsorption of DB15 azo dyes of the working membrane forms was drawn. This graph showing the relation between log q_e and log C_e was given in **Figure 9**.

$$log\, q_e = \log K_F + \frac{1}{n} log\, C_e \tag{3}$$

The Langmuir adsorption isotherm is generally used to describe the maximum adsorption capacity of an adsorbent. qm and b values were calculated from the above equation. b is a constant related to adsorption net enthalpy (L/mg), and qm is the amount of adsorbed material (mg/g) in the unit weight of the adsorbent to form a single layer at the surface. In the Langmuir isotherm study, the highest q_m value was obtained LS-ZnO/Fe_3O_4 membrane form

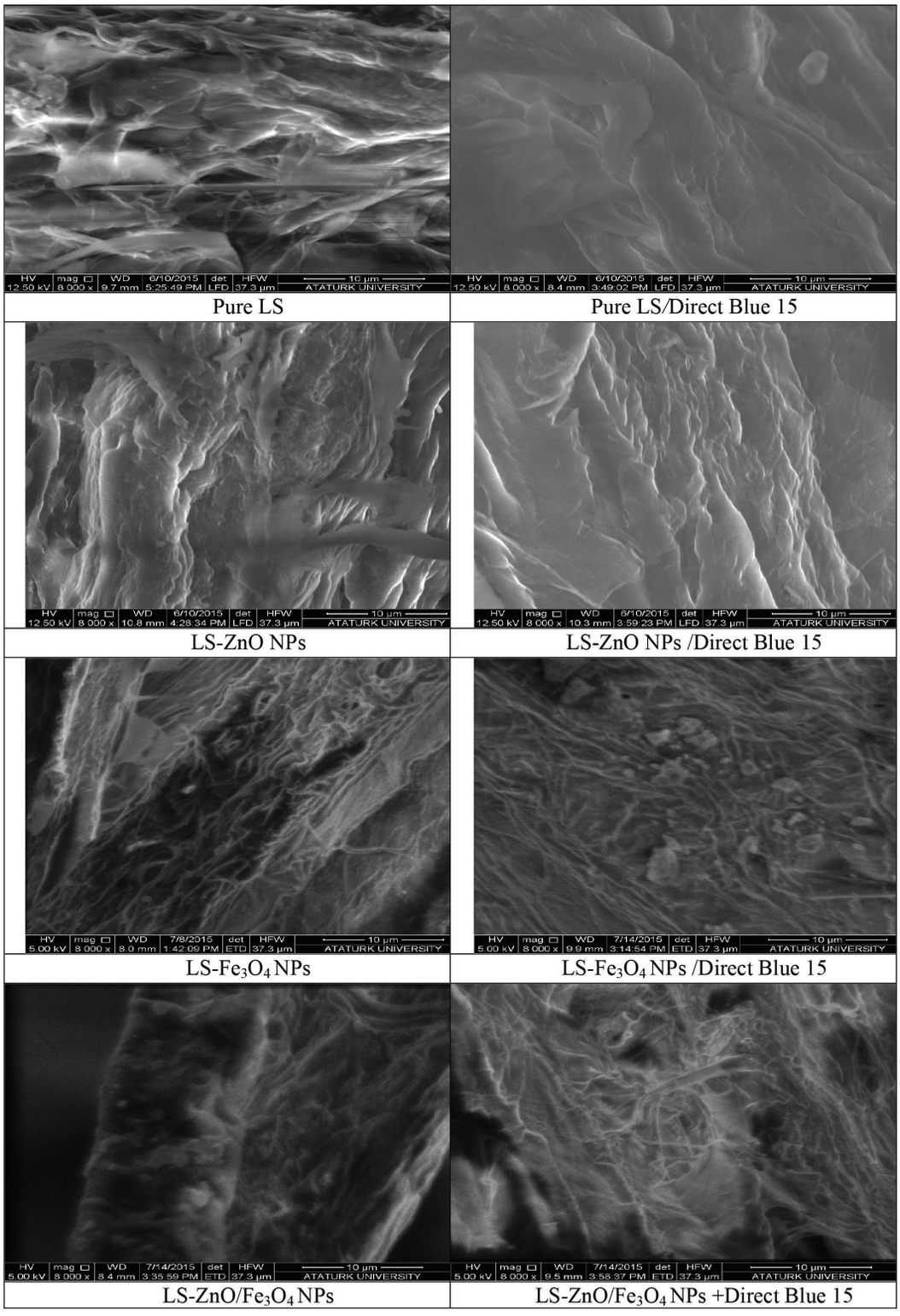

Figure 7. SEM images of adsorption of DB15 azo dye with membrane forms.

with 274.6 mg/g and the lowest q_m value was obtained with pure LS membrane form with 45.0 mg/g. The highest b value was achieved with the pure LS membrane form with 1.186 L/mg and the LS-ZnO/Fe_3O_4 NPs membrane form with a minimum b value of 0.06 L/mg. High

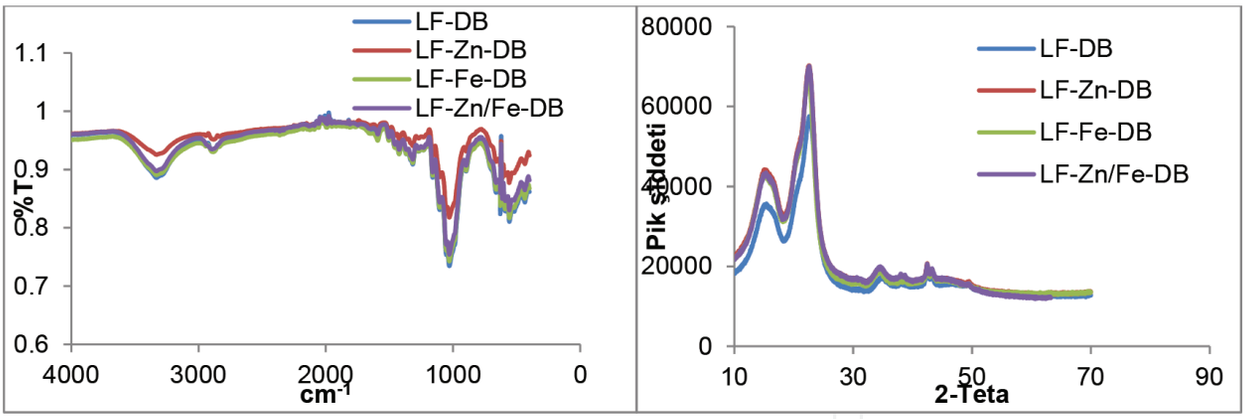

Figure 8. FT-IR and XRD spectrums of adsorption of DB15 azo dye with membrane forms.

correlation coefficient R^2 (0.9605) was provided with Langmuir model, the linear form application for LS-Fe_3O_4. This indicates that the sorption system of Langmuir isotherm provides a good model for this membrane form (**Table 4**).

Freundlich isotherm model is an empirical relationship that defines the adsorption of solubles from a liquid to a solid surface and assumes that there are different areas with several adsorption energies. Freundlich constants are related to the sorption capacity of the adsorbent (mg/g) and adsorption energy. In the Freundlich model, K_F and n are constants that show the adsorption capacity and intensity, respectively. High K_F and n values indicate high adsorption capacity and magnitude of n value is an indication of the suitability of adsorption. The LS-ZnO NPs membrane form with 2.65 values of n had a good adsorption capacity relative to the Freundlich isotherm. The pure LS membrane form is quite advantageous according to R^2 (0.9885) (**Table 4**).

3.7. Reaction kinetics of first and second order

The adsorption kinetics of DB15 azo dye with LS, LS-ZnO NPs, LS-Fe_3O_4 NPs, LS-ZnO/Fe_3O_4 NPs membrane forms and were investigated against 10, 25, 50, 100, and 200 mg/L concentrations of dye solutions. To determine the adsorption constants, first order conformity to reaction

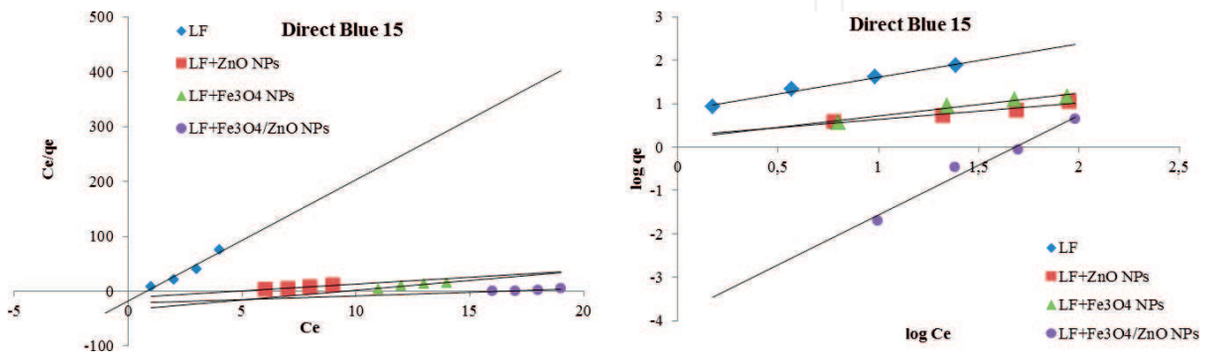

Figure 9. Langmuir and Freundlich adsorption isotherm for DB15 azo dye adsorption with membrane forms.

	DB15			
	LS	**LS-ZnO**	**LS-Fe_3O_4**	**LS-ZnO/Fe_3O_4**
Langmuir constants				
q_m (mg/g)	45.0	48.6	128.1	274.6
b(L/mg)	1.186	0.216	0.103	0.06
R^2	0.9503	0.9371	0.9605	0.7641
Freundlich constants				
K_F (mg/g) $(L/mg)^{1/n}$	6.85	1.84	1.53	1.36×10^{-4}
n	1.29	2.65	1.899	0.44
R^2	0.9885	0.9378	0.9637	0.9716

Table 4. Langmuir and Freundlich isotherm parameters.

kinetics was investigated. For this purpose, the time-dependence of $\ln(q_e - q_t)$ was plotted and R^2 values were calculated for 10, 25, and 50 mg/L concentrations of dye (**Table 5**).

The k_1 constant is calculated using the first order reaction equation given below:

$$\ln(q_e - q_t) = \ln q_e - k_1 t \tag{4}$$

Then, its suitability of second-order reaction kinetics was investigated to calculate the adsorption constants of DB15 azo dye. (t/qt) depicting the time dependence graphs were plotted and R^2 values for 10, 25, and 50 mg/L concentrations of DB15 azo dyes were calculated (**Table 5**).

The second-order reaction equation is used to calculate the k_2 constant and all calculated values ($qe_{experimental}$, $qe_{calculated}$, k_1, k_2, R^2) for adsorption of azo dye DB15 are shown in **Table 5**.

When **Table 5** is examined, there is high difference between values of $qe_{experimental}$ and $qe_{calculated}$ in the reaction kinetics of the first- and second-order in dye adsorption with pure LS membrane form. Furthermore, when the R^2 values are examined, it is clear that the second order is inadequate. There is lower difference than the other concentration between values of $qe_{experimental}$ and $qe_{calculated}$ in reaction kinetics of the second order in adsorption of azo dye at a concentration of 10 mg/L with the LS-ZnO NPs membrane form. However, when we take into account the R^2 values, there is a compatibility with the first-order reaction kinetics. We see that the adsorption of azo dye at 25 mg/L concentration with Fe_3O_4 NPs-loaded membrane forms is more appropriate for the second-order reaction kinetics in terms of R^2 values.

3.8. Calculation of thermodynamic parameters

Plots of LnK_L against 1/T obtained in adsorption experiments with membrane forms of DB15 azo dye are given in **Figure 10**.

Values for ΔG° Gibbs free energy, ΔH° enthalpy change and ΔS° entropy thermodynamic parameters for membrane forms used in the adsorption of DB15 azo dyes are given in **Table 6**.

DB15								
Adsorbent	**Initial dye conc.**	**qe_{exp} (mg/g)**	**First order**			**Second order**		
			k_1 (L/min)	**qe_{cal} (mg/g)**	**R^2**	**k_2 (g/mg min)**	**qe_{cal} (mg/g)**	**R^2**
LS	10	8.8	0.034	0.845	0.9954	5.77×10^{-4}	16.53	0.9751
	25	12.6	0.030	0.978	0.9977	2.27×10^{-3}	20.70	0.9955
	50	33.6	0.0.28	1.296	0.9873	6.8×10^{-5}	96.15	0.6882
LS-ZnO NPs	10	9.1	0.053	0.809	0.9974	2.63×10^{-3}	12.03	0.9702
	25	17.1	0.038	1.071	0.9986	1.03×10^{-3}	26.46	0.9923
	50	49.65	0.049	1.395	0.9744	8.78×10^{-5}	95.24	0.9547
LS-Fe_3O_4 NPs	10	8.6	0.055	0.949	0.925	2.03×10^{-3}	13.14	0.9912
	25	22.7	0.049	1.113	0.9983	1.45×10^{-3}	27.25	0.991
	50	44.3	0.054	1.414	0.9603	1.48×10^{-4}	76.33	0.9654
LS-ZnO/Fe_3O_4 NPs	10	8.9	0.047	0.839	0.9821	2.83×10^{-3}	12.76	0.9971
	25	24.0	0.039	1.075	0.9494	1.23×10^{-3}	29.94	0.9537
	50	48.6	0.054	1.400	0.9715	2.54×10^{-4}	67.57	0.9876

Table 5. First- and second-order adsorption rate constants in DB15 azo dye removal.

ΔG° values decreased as the temperature increases in adsorption of DB15 azo dye with all membrane forms. This shows an increasing tendency in the feasibility and spontaneity of DB15 azo dye adsorption. The fact that ΔG° has negative values means that the adsorption of DB15 azo dye is spontaneously. The negative values of ΔH° confirm the exothermic structure of the adsorption process. Therefore, the adsorption of DB15 azo dye with membranes formed by the use of

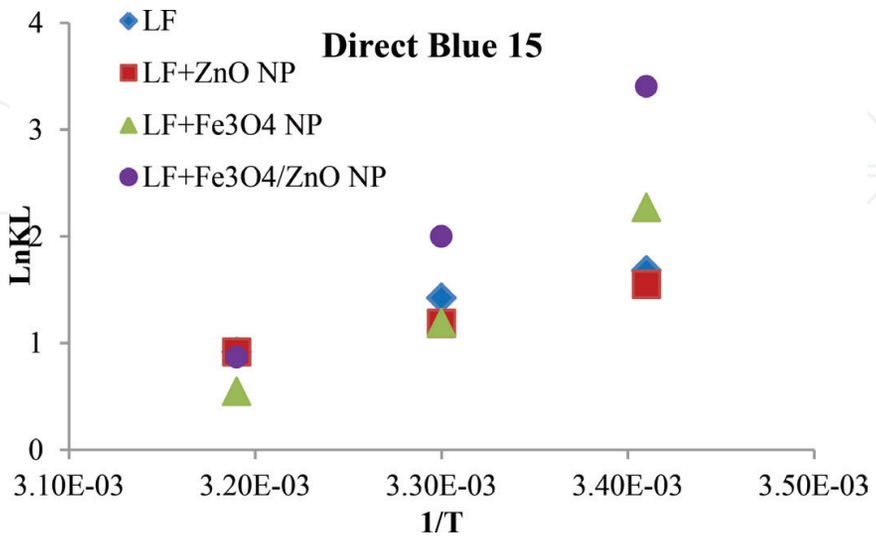

Figure 10. Thermodynamic kinetics graph for adsorption of DB15 azo dye with formed membrane forms.

DB15			
	ΔG° (kJ/mol K)	**ΔH° (kJ/mol)**	**ΔS° (kJ/mol)**
LS 20°C	−24235.32	−417.7	−84.14
LS 25°C	−24656.02		
LS 30°C	−25076.72		
LS-ZnO NPs 20°C	−19855.73	−346.62	−68.95
LS-ZnO NPs 25°C	−20200.48		
LS-ZnO NPs 30°C	−20545.23		
LS-Fe_3O_4 NPs 20°C	−58727.95	−941.5	203.65
LS-Fe_3O_4 NPs 25°C	−59746.20		
LS-Fe_3O_4 NPs 30°C	−60764.45		
LS-ZnO/Fe_3O_4 NPs 20°C	−86188.31	−1386.46	298.89
LS-ZnO/Fe_3O_4 NPs 25°C	−87682.76		
LS-ZnO/Fe_3O_4 NPs 30°C	−89177.21		

Table 6. Calculated thermodynamic constants.

LS and nanoparticle is a natural chemical. Positive values of ΔS° indicate increasing disorder and randomness at the solid solution interface of the adsorbent and DB15 azo dye [49]. This was observed in membrane forms immobilized with Fe_3O_4 NPs (**Table 6**).

4. Conclusion

In this study on remediation, the possibilities offered by the environment are evaluated. ZnO and Fe_3O_4 NPs were produced by green synthesis with catalyzed peroxidase enzyme partially purified from *Euphorbia amygdaloides* plant. In this phase of the study, a new plant source was presented to literature for the green synthesis of nanoparticles. It has also been shown that produced nanoparticles may play an active role in dye adsorption. The synthesis of this plant with other nanoparticles will be further studied.

LS is a natural plant that can grow in many countries, can be used for many purposes, and has recently undergone a lot of research. In this study, nanoparticles were immobilized successfully on this material. In this way, it is aimed to prevent the nanoparticles accumulation in the environment and the creation of a separate pollution. Adsorption of DB15, a carcinogenic azo dye, was studied with nanoparticle-loaded membrane forms. Optimization, characterization, kinetic, thermodynamic studies demonstrated effectiveness of the membrane forms used in dye adsorption. For this reason, we can easily say that this work will be a source for commercialized membrane systems in the future.

Acknowledgements

This research was performed under the project numbered 115Z810 and supported by the Scientific and Technical Research Council of Turkey (TUBITAK). The authors acknowledge the support of TUBITAK, Turkey for this work.

Author details

Hayrunnisa Nadaroglu[1,2]*, Semra Cicek[3], Hicran Onem[2] and Azize Alayli Gungor[4]

*Address all correspondence to: hnisa25@atauni.edu.tr

1 Department of Food Technology, Erzurum Vocational Training School, Ataturk University, Erzurum, Turkey

2 Department of Nano-Science and Nano-Engineering, Faculty of Engineering, Ataturk University, Erzurum, Turkey

3 Department of Agricultural Biotechnology, Faculty of Agriculture, Ataturk University, Erzurum, Turkey

4 Department of Chemical Technology, Erzurum Vocational Training School, Ataturk University, Erzurum, Turkey

References

[1] Majcen-Le Marechal A, Slokar YM, Taufer T. Decoloration of chlorotriazine reactive azo dyes with H_2O_2/UV. Dyes and Pigments. 1997;**33**:281-298

[2] Shaul GM, Lieberman RJ, Dempsey CR, Dostal KA. Treatability of water soluble azo dyes by the activated sludge process. Proceedings of the Industrial Wastes Symposia WPCF. 1986:1-18

[3] Gomes JR. Estrutura e Propriedades dos Corantes. Braga, Portugal: Barbosa e Xavier Lda; 2001

[4] Pereira L, Alves M. Dyes—Environmental impact and remediation. In: Malik A, Grohmann E, editors. Environmental Protection Strategies for Sustainable Development, Strategies for Sustainability. Netherlands: Springer; 2012. pp. 111-154

[5] Balan DSL. Biodegradação e toxicidade de efluentes têxteis. Revista Brasileira de Técnicos Têxteis - ABTT. 2009;**1**(1):16-18

[6] Gupta VK, Khamparia S, Tyagi I, Jaspal D, Malviya A. Decolorization of mixture of dyes: A critical review. Global Journal of Environmental Science and Management. 2015;**1**:71-94

[7] Campos-Takaki GM, Vilar Junior JC, Cavalcanti DL, Alves da Silva CA, Andrade RFS. Decolorization of black B azo dye by *Pseudomonas aeruginosa*. International Journal of Current Microbiology and Applied Sciences. 2015;**4**(7):720-728

[8] Gunasekaran P, Puvaneswari N, Muthukrishnan J. Toxicity assessment and microbial degradation of azo dyes. Indian Journal of Experimental Biology. 2006;**44**:618-626

[9] Clarke EA, Anliker R. Organic dyes and pigment. In: Hutzinger O, editor. The Handbook of Environmental Chemistry. 3. A. Anthropogenic Compounds. United States: Springer-Verlag; 1980. pp. 1-215

[10] Ventura-Camargo BC, Marin-Morales MA. Azo dyes: Characterization and toxicity—A review. Textiles and Light Industrial Science and Technology (TLIST). 2013;**2**(2):85-103

[11] Robinson T, Mcmullan G, Marchant R, Nigam P. Remediation of dyes in textile effluent: A critical review on current treatment technologies with a proposed alternative. Bioresource Technology. 2001;**77**:247-255

[12] Jadhav JP, Parshetti GK, Kalme SD, Govindwar SP. Decolourization of azo dye methyl red by *Saccharomyces cervisiae* MTCC 463. Chemosphere. 2007;**68**:394-400

[13] Karn B, Kuiken T, Otto M. Nanotechnology and in situ remediation: A review of the benefits and potential risks. Environmental Health Perspectives. 2009;**117**:1823-1831

[14] Nam S, Tratnyek PG. Reduction of azo dyes with zero-valent iron. Water Research. 2000;**34**:1837-1845

[15] Gupta N, Singh HP, Sharma RK. Metal nanoparticles with high catalytic activity in degradation of methyl orange: An electron relay effect. Journal of Molecular Catalysis A: Chemical. 2011;**335**:248-252

[16] Wang JQ, Liu YH, Chen MW, Louzguine-Luzgin DV, Inoue A, Perepezko JH. Excellent capability in degrading azo dyes by MgZn-based metallicglass powders. Scientific Reports. 2012;**2**:418-423

[17] Vidhu VK, Philip D. Catalytic degradation of organic dyes using biosynthesized silver nanoparticles. Micron. 2014;**56**:54-62

[18] Philip D, MeenaKumari M. Degradation of environment pollutant dyes using phytosynthesized metal nanocatalysts. Spectrochimica Acta Part A: Molecular and Biomolecular Spectroscopy. 2015;**135**:632-638

[19] Rahman N, Abedin Z, Hossain MA. Rapid degradation of azo dyes using nano-scale zero valent iron. American Journal of Environmental Sciences. 2014;**10**(2):157-163

[20] Adams LK, Lyon DY, Alvarez PJJ. Comparative ecotoxicity of nanoscale TiO_2, SiO_2 and ZnO water suspensions. Water Research. 2006;**40**:3527-3532

[21] Lovern SB, Strickler JR, Klaper R. Behavioral and physiological changes in *Daphnia magna* when exposed to nanoparticle suspensions (titanium dioxide, nano-C_{60} and $C_{60}H_xC_{70}H_x$). Environmental Science & Technology. 2007;**41**(12):4465-4470

[22] Saeed A, Iqbal M. Loofa (Luffa cylindrica) sponge: Review of development of the biomatrix as a tool for biotechnological applications. Biotechnology Progress. 2013;**29**:573-600

[23] Güngör AA, Demir N, Demir Y. Purification of peroxidase from latex of euphorbia (*Euphorbia amygdaloides*) and investigation of kinetic properties. Asian Journal of Chemistry. 2008;**20**(1):477-482

[24] Su CH, Liu DZ, Jiang PL, Chien MY, Sheu MT, Huang YY, Chen MH. Dried fruit of the *Luffa sponge* as a source of chitin for applications as skin substitutes. BioMed Research International. 2014;**2014**:1-9 [article ID 458287]

[25] Converso DA, Fernandez ME. Peroxidase isozymes from wheat germ: Purification and properties. Phytochemistry. 1995;**40**:1341-1345

[26] Billaud C, Louarme L, Nicolas J. Comparison of peroxidases from barley kernel (*Hordeum vulgare* L.) and wheat germ (*Triticum aestivum* L.): Isolation and preliminary characterization. Journal of Food Biochemistry. 1999;**23**:145-172

[27] Chen Z, Mabrouk PA. Isolation and purification of soybean peroxidase from "Montsew" Chinese soybeans. National Undergraduate Research Clearinghouse; 2000. pp. 2-7

[28] Dicko MH, Gruppen H, Hilhorst R, Voragen AG, Berkel WJV. Biochemical characterization of the major sorghum grain peroxidase. FEBS Journal. 2006;**273**:2293-2307

[29] Suzuki T, Honda Y, Mukasa Y, Kim SJ. Characterization of peroxidase in buckwheat seed. Phytochemistry. 2006;**67**:219-224

[30] Geetha MS, Nagabhushana H, Shivananjaiah HN. Green mediated synthesis and characterization of ZnO using *Euphorbia Milli* latex as fuel. IJSR. 2016;**5**(4):158-163

[31] Nasrollahzadeh M, Sajadi SM. Preparation of Pd/Fe_3O_4 nanoparticles by use of *Euphorbia stracheyi Boiss* root extract: A magnetically recoverable catalyst for one-pot reductive amination of aldehydes at room temperature. Journal of Colloid and Interface Science. 2016;**464**:147-152

[32] Slman AA. Antibacterial activity of ZnO nanoparticle on some gram-positive and gram-negative bacteria. Iraq. Journal de Physique. 2012;**10**(18):5-10

[33] Ng JCY, Cheung WH, McKay G. Equilibrium studies for the sorption of lead from effluents using chitosan. Chemosphere. 2003;**52**:1021-1030

[34] Sharma P, Sreenivas K, Rao KV. Analysis of ultraviolet photoconductivity in ZnO films prepared by unbalanced magnetron sputtering. JJAP. 2003;**93**:3963-3970

[35] Rahman OU, Mohapatra SC, Ahmad S. Fe_3O_4 inverse spinal super paramagnetic nanoparticles. Materials Chemistry and Physics. 2012;**132**:196-202

[36] Nagarajan S, Kuppusamy KA. Extracellular synthesis of zinc oxide nanoparticle using seaweeds of gulf of Mannar, India. Journal of Nanbiotechnology. 2013;**11**:39

[37] Manouchehr N, Mehriana A, Reza L, Rostami MH. The optimum conditions for synthesis of Fe_3O_4/ZnO core/shell magnetic nanoparticles for photodegradation of phenol. IJEHSE. 2014;**12**(21):1-6

[38] Gnanasangeetha D, Sarala TD. Benign ZnO nanoparticle as a practical adsorbent for removal of As^{3+} embedded on activated silica using *Ocimum Sanctum*. Discovery. 2014;**16**(46):33-41

[39] Davar F, Majedi A, Mirzaei A. Green synthesis of ZnO nanoparticles and its application in the degradation of some dyes. Journal of the American Ceramic Society. 2015;**98**(6):1739-1746

[40] Rasool K, Lee DS. Effect of ZnO nanoparticles on biodegradation and biotransformation of co-substrate and sulphonated azo dye in anaerobic biological sulfate reduction processes. International Biodeterioration & Biodegradation. 2016;**109**:150-156

[41] Sharma ACD, Sun Q, Li J, Wang Y, Suanon F, Yang J, Yu CP. Decolorization of azo dye methyl red by suspended and co-immobilized bacterial cells with mediators anthraquinone-2,6-disulfonate and Fe_3O_4 nanoparticles. International Biodeterioration & Biodegradation. 2016;**112**:88-97

[42] Sun JH, Shi SH, Lee YF, Sun SP. Fenton oxidative decolorization of the azo dye direct blue 15 in aqueous solution. Chemical Engineering Journal. 2009;**155**(3):680-683

[43] Weng CH, Lin YT, Chang CK, Liu N. Decolourization of direct blue 15 by Fenton/ultrasonic process using a zero-valent iron aggregate catalyst. Ultrasonics Sonochemistry. 2013;**20**(3):970-977

[44] Zhan Y, Zhou X, Fu B, Chen Y. Catalytic wet peroxide oxidation of azo dye (direct blue 15) using solvothermally synthesized copper hydroxide nitrate as catalyst. Journal of Hazardous Materials. 2011;**187**(1-3):348-354

[45] Kesraoui A, Moussa A, Ben Ali G, Seffen M. Biosorption of Alpacide blue from aqueous solution by lignocellulosic biomass: *Luffa cylindrica* fibers. Environmental Science and Pollution Research. 2016;**23**(16):15832-15840

[46] Siquera G, Bras J, Follain N, Belbekhouche S, Marais S, Dufresne A. Thermal and mechanical properties of bionanocomposites reinforced by *Luffa cylindrica* cellulose nanocrystals. Carbohydrate Polymers. 2013;**91**:711-717

[47] Tong Y, Zhao S, Ma J, Wang L, Zhang Y, Gao Y, Xie YM. Improving cracking and drying shrinkage properties of cement mortar by adding chemically treated luffa fibres. Construction and Building Materials. 2014;**71**:327-333

[48] Chen C, Luo Wen J, Tong Q. Elemental analysis, chemical composition, cellulose crystallinity, and FT-IR spectra of *Toona sinensis* wood. Abrégé en. Monatshefte fuer Chemie. 2014;**145**(1):175-185

[49] Kalkan E, Nadaroglu H, Celebi N, Tozsin G. Removal of textile dye reactive black 5 from aqueous solution by adsorption on laccase-modified silicafume. Desalination and Water Treatment. 2014;**52**(31-33):6122-6134

IntechOpen